

On the effect of pressure on intrinsic flame instabilities in lean hydrogen-air mixtures – Part II: Experimental investigation based on OH-PLIF technique

P. Katzy, J. Hasslberger and T. Sattelmayer
Lehrstuhl für Thermodynamik, Technische Universität München (TUM)
Garching, Germany

1 Introduction

This work aims to quantify the effect of pressure on flame front wrinkling caused by intrinsic flame instabilities in lean hydrogen-air explosions. Work concerning pressure dependency was conducted (e.g. by Kobayashi et al. [1] or Dinkelacker et al. [2]), however only for fuels other than pure hydrogen, like methane, ethylene, propane or methane/hydrogen blends. Furthermore, these flames were investigated for a stationary case under conditions with high turbulence intensity compared to this case, where the initial turbulence level is assumed to be negligible.

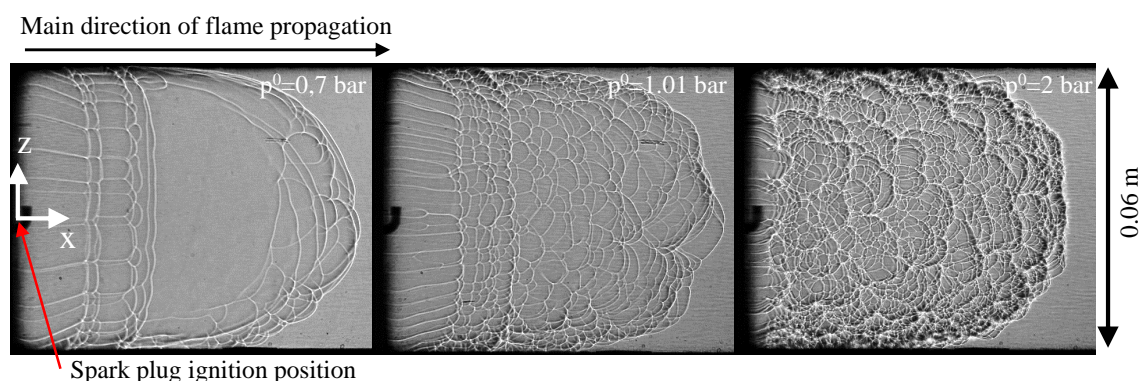


Figure 1: Shadowgraphy images of hydrogen-air flames with a hydrogen concentration of 13 % propagating from left to right under variation of initial pressure p^0 . The images were taken at comparable distances of the flame tip from the ignition position.

In Fig. 1 shadowgraphy images of lean hydrogen-air flames are compared against each other. The hydrogen concentration in all three cases is 13 % and the images are taken at comparable distances of the flame tip from the ignition position. The mixture is ignited through a spark plug (NGK BKR6EIX-LPG) at the position $(x = 0, y = 0, z = 0)$. The images show that each flame develops to a wrinkled flame front with varying intensities. Due to the negligible turbulence level of the mixture prior to ignition, wrinkling of the flame front is assumed to be mainly caused by intrinsic flame instabilities, like the Landau-Darrieus and the thermal-diffusive instability, the latter playing a predominant role in the investigated case [8]. Three cases with increasing initial pressure p^0 are depicted in Fig. 1. It shows, that the intensity of flame front wrinkling increases with initial pressure p^0 .

The goal of this work is to improve hydrogen-air combustion CFD modeling on under-resolved grids in the context of Unsteady Reynolds-Averaged Navier-Stokes simulations (URANS). In this approach, an effect like the observed flame front wrinkling in Fig. 1 cannot be resolved and must be modeled. Using a transport equation of the averaged reaction progress variable c is a widely-used approach to simulate premixed flames. This equation must be closed by modeling of the averaged source term, e.g. by the gradient approach suggested by Zimont et al. [3]:

$$\bar{\omega}_c = \bar{\rho}_u s_t |\nabla \bar{c}| \quad (1)$$

However, this equation is unclosed itself which is why a correlation for the turbulent flame speed s_t must be formulated. In this work, a closure based on Damköhler's work [4] is used to capture the effect of the increased flame front surface:

$$s_t = \Xi_{3D} \cdot s_l \approx \frac{A_{\text{wrinkled}}}{A_{\text{smooth}}} \cdot s_l \quad (2)$$

A_{wrinkled} represents the wrinkled flame surface, whereas A_{smooth} corresponds to a hypothetical smooth flame surface without small-scale wrinkling. In Tab. 1 the used experimental and numerical techniques are summarized, showing the complementary methodological approach employed at TUM in the field of explosion research. The work presented in the following sections builds on the Direct Numerical Simulation (DNS) results of Part I of this study and experimental Planar Laser-Induced Fluorescence measurements of the OH radical (OH-PLIF) conducted within this Part. The data obtained with these fundamentally different approaches is used to formulate the observed dependency of flame front augmentation observed with increasing initial pressure.

Table 1: Complementary explosion analysis methods employed at TUM

	Experiment	Simulation
Macroscopic	Conventional: Pressure transducer, Photo diodes	3D, URANS, Turbulent Flame speed Closure, CFX
Microscopic	Optical: Shadowgraphy, OH-PLIF	2D, DNS, Detailed chemistry, OpenFOAM

2 Experimental setup and data evaluation

The test facility used in this work is the entirely closed laboratory-scale GraVent explosion channel [5], depicted schematically in a sectional view in the left part of Fig. 2. The channel has a rectangular cross-section (not shown here) with a width of 0.3 m, a height of 0.06 m (shown in Fig. 1) and a length of 1.3 m in the current setup. The desired hydrogen concentration prior to an experiment is realized with the partial pressure method. The mixture is ignited at the $(x, y, z) = \vec{0}$ position after a waiting time of 60 s past the injection of hydrogen to ensure a negligible initial turbulence level and a homogeneous distribution of hydrogen. After the ignition, the flame front propagates through the channel until it reaches the channel end plate at the distance of $x = 1.3$ m. The maximum optically accessible area covers a distance $x = 0$ m to $x = 0.23$ m. In the current work the flame propagation is recorded up to a distance of approximately 0.16 m.

In the right part of Fig. 2 the z-type shadowgraphy- and OH-PLIF-setup are shown. The applied laser system is a combination of a Nd:YVO4 solid state pump laser (Innoslab IS8II) and a tunable dye laser

(Sirah Credo Dye). The dye laser provides UV-light with the desired wave length of 282.94 nm for excitation of OH-radicals from the $X^2\Pi_i$ band to the $A^2\Sigma^+$ band [6]. The high speed cameras used are the Photron SAX for the shadowgraphy- and the Photron SAX2 for the OH-PLIF-measurements allowing simultaneous measurements with a repetition rate of 20 kHz at a resolution of 1024x512 pixels. Additionally, an UVi 1850B-10-S20 image intensifier is used for OH-PLIF measurements.

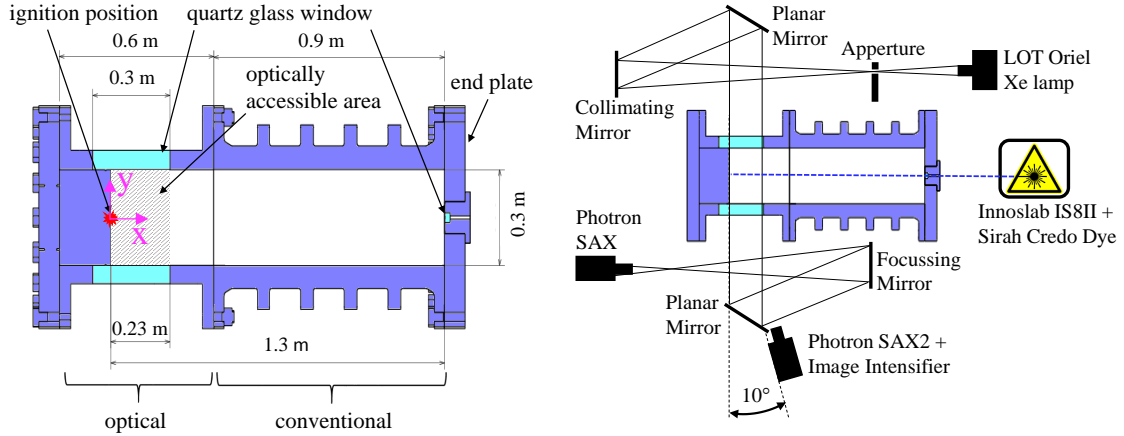


Figure 2: Left: Sectional top view of the GraVent facility. Right: Setup of shadowgraphy- and OH-PLIF-technique used in this work.

Table 2 summarizes the experimentally and numerically investigated cases at a hydrogen concentration of 13 %. In the experiments three initial pressure levels (0.7 bar, 1.01 bar and 2 bar) were investigated. The 0.5 bar pressure level was solely investigated in terms of DNS. The non-line-of-sight integrated OH-PLIF data for the three experimentally investigated cases was used to determine two-dimensional wrinkling factors Ξ_{2D} based on the comparison of the wrinkled (L_{wrinkled}) and smooth (L_{smooth}) flame front length:

$$\Xi_{2D} = \frac{L_{\text{wrinkled}}}{L_{\text{smooth}}} \quad (3)$$

Table 2: Case overview

No.	X_{H_2} [%]	p^0 [bar]	$n \cdot 10^6$	Sc_k	Method
1 (ref.)	13	1.01	12.19	Individual	DNS + PLIF
2	13	1.01	7.8	Individual	DNS
3	13	1.01	21.67	Individual	DNS
4	13	1.01	12.19	Identical ($Sc_k = 1.0$)	DNS
5	13	0.5	12.19	Individual	DNS
6	13	2.0	12.19	Individual	DNS + PLIF
7	13	0.7	12.19	Individual	DNS + PLIF

In the left part of Fig. 3 the detected flame fronts in an OH-PLIF image for the reference case 1 are shown. For the evaluation of the wrinkled flame front L_{wrinkled} an automated Matlab routine is used, based on the binarization of raw OH-PLIF images [7]. The hypothetical flame front L_{smooth} is obtained through reproduction of the wrinkled flame front on a quadratic grid by means of a spline with five sampling points and the same top and bottom points as the detected wrinkled flame front L_{wrinkled} . The distance between the sampling points should be chosen sufficiently high, so that small scale wrinkling

cannot be resolved. That way, only the front length due to the macroscopic shape of the flame is captured. In the next step the intersections between the spline and the grid are connected linearly to assure the detection of a flame front without wrinkles. The evaluation grid size in this work was chosen to be 7.5 mm corresponding to the computational grid size in a hypothetical under-resolved CFD-simulation. In the last step the flame front wrinkling factor Ξ_{2D} is calculated for every recorded image, allowing the investigation of the temporal development of Ξ_{2D} . In the right part of Fig. 3 the temporal development for the reference case (Tab. 2, No. 1) is depicted. The curves for L_{wrinkled} and L_{smooth} exhibit a characteristic shape due to the change of the macroscopic curvature of the flame front. In regime A the flame front length is increasing until the hemispherical flame kernel reaches the channel's top and bottom walls. The decreasing values in regime B are due to flattening of the macroscopic shape of the flame. Regime C shows a comparably constant behavior of both flame front lengths until the flame leaves the recorded area. This behavior is resulting from the predominantly constant macroscopic shape of the propagating flame front, which is why the two-dimensional flame wrinkling factor is evaluated by averaging Ξ_{2D} in this regime.

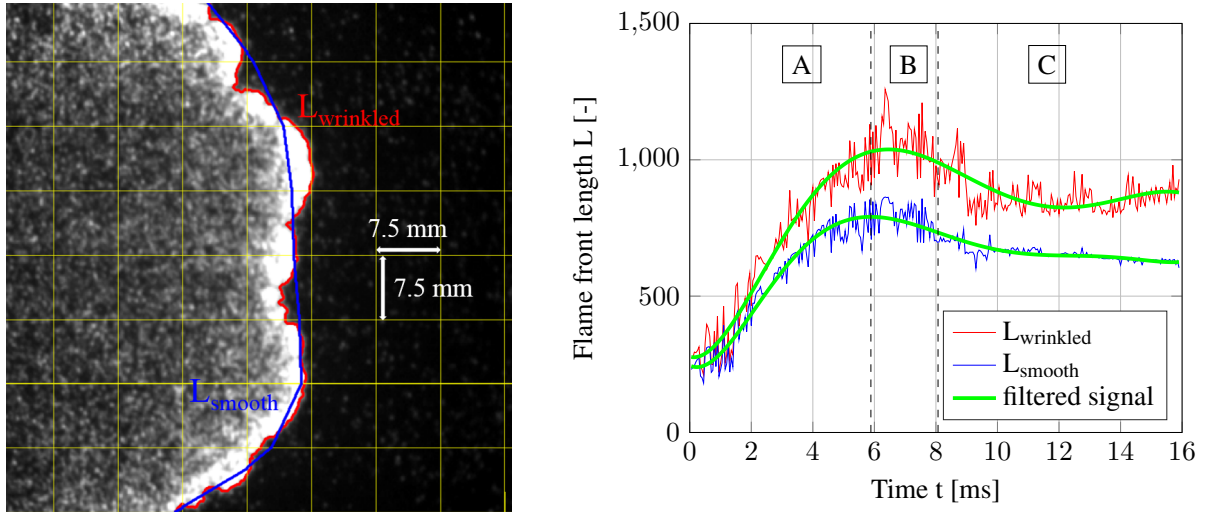


Figure 3: Left: OH-PLIF image with detected wrinkled (L_{wrinkled}) and smooth (L_{smooth}) flame fronts. Right: Temporal evolution of detected flame front lengths.

These wrinkling factors are not accounting for wrinkling perpendicular to the image plane due to the inherent two-dimensionality of the OH-PLIF technique. The flame fronts in Fig. 1 indicate that wrinkling has no preferred direction and develops similarly in vertical and horizontal direction on the flame surface. Based on this observation, wrinkling of the flame front is assumed to be identical in both directions which leads to the following formulation of the wrinkling factor:

$$\Xi_{3D} = \Xi_{2D}^2. \quad (4)$$

3 Results and discussion

In Fig. 4 post-processed OH-PLIF recordings for cases 1, 6 and 7 are shown. The structure of the wrinkled flame front alters under variation of initial pressure p^0 . According to the observations in Fig. 1 the change of the cell size can also be identified in OH-PLIF recordings with varying pressure.

The goal of this work is to quantitatively determine the increase of flame front area due to variation of pressure by the factor β_{Ξ} :

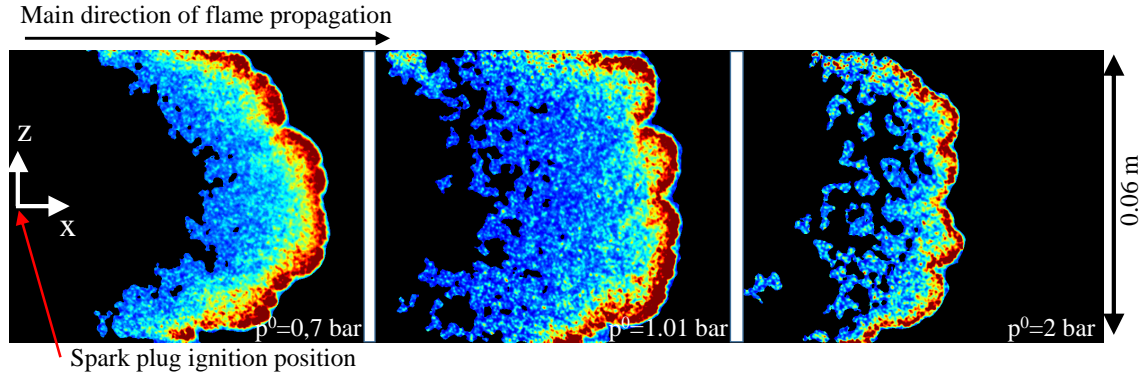


Figure 4: OH-PLIF images under variation of initial pressure p^0 . The OH-PLIF signal is colored according to its intensity in the raw images. Red: high intensity; blue: low intensity; black: no signal detected. Main direction of flame propagation from left to right.

$$\Xi_{3D} = \Xi_{2D}^2 = f(\text{Le}, p) = f(\text{Le}) \cdot f(p) = f(\text{Le}) \Big|_{p_{\text{ref}}} \cdot \left(\frac{p}{p_{\text{ref}}} \right)^{\beta_{\Xi}} \quad (5)$$

To meet this goal DNS and OH-PLIF data under variation of initial pressure are evaluated and the results are compared with each other. For both data sets the identical evaluation method, described in section 2, was used. The evaluated DNS data consists of flame fronts corresponding to four pressure levels (0.5 bar, 0.7 bar, 1.01 bar and 2 bar) according to cases 1, 5, 6 and 7. The evaluation of the DNS data was conducted in the front part of the computational domain where the pressure rise during the simulation is assumed to be small. The OH-PLIF data encompasses three pressure levels (0.7 bar, 1.01 bar and 2 bar) according to cases 1, 6 and 7. Due to statistical scattering of the experimental results, three values for Ξ_{3D} for each pressure level are provided. The summarized results are shown in Fig. 5 where Ξ_{3D} is plotted over initial pressure p^0 . An increase of Ξ_{3D} with increasing initial pressure p^0 can be identified for experimentally and numerically determined values. Furthermore, the values of the determined wrinkling factors are in good agreement under varying pressure. The fitted power law function according to Eq. 5 leads to a factor $\beta_{\Xi} = 0.18$.

4 Conclusion and outlook

The dependency of flame front wrinkling caused by intrinsic laminar instabilities under pressure variation was investigated in a complementary approach. High-speed OH-PLIF measurements and DNS simulations of propagating lean hydrogen-air flames were conducted. In the investigated lean hydrogen-air case both intrinsic instability mechanisms are superimposed, however the thermal-diffusive instability is dominantly influencing the cellular structure. A reduction of the thermal-diffusive cell size was observed with increasing initial pressure. The quantitative evaluation of the data showed an increase of the wrinkling factor under increasing normalized pressure to the power of $\beta_{\Xi} = 0.18$. The dependency identified leads to the conclusion that the pressure influence on flame front wrinkling of a propagating lean hydrogen-air flame should not be neglected.

In the next step the determined dependency must be incorporated in an under-resolved CFD subgrid model and simulations must be compared against global experimental data, e.g. flame speed trajectories.

The presented work is funded by the German Federal Ministry of Economic Affairs and Energy (BMWi) on the basis of a decision by the German Bundestag (project no. 1501485) which is gratefully acknowledged.

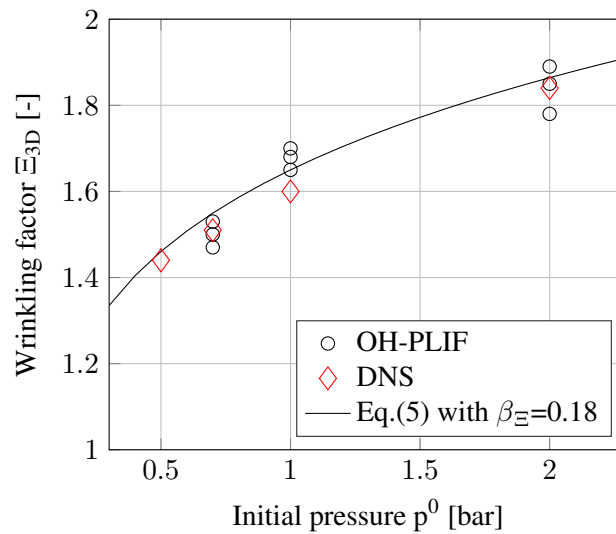


Figure 5: Evaluated values for Ξ_{3D} under variation of initial pressure p^0 : DNS simulations (red diamonds) and OH-PLIF measurements (black circles)

References

- [1] Kobayashi, H., Kawabata, Y. and Maruta, K. (1998). Experimental Study on General Correlation of Turbulent Burning Velocity at High Pressure. Symposium (International) on Combustion 27(1): 941 - 948.
- [2] Dinkelacker, F., Manickam, B. and Muppala, S.P.R. (2011). Modelling and Simulation of Lean Premixed Turbulent Methane/Hydrogen/Air Flames with an Effective Lewis Number Approach. Combustion and Flame 158(19): 1742 - 1749.
- [3] Zimont, V., Polifke, W., Bettelini, M. and Weisenstein, W. (1998). An Efficient Computational Model for Premixed Turbulent Combustion at High Reynolds Numbers Based on a Turbulent Flame Speed Closure. Transactions of the ASME 120: 526 - 532.
- [4] Damköhler, G. (1940). Der Einfluss der Turbulenz auf die Flammgeschwindigkeit in Gasgemischen. Zeitschrift für Elektrochemie und angewandte physikalische Chemie 46: 601 - 652.
- [5] Vollmer, K. (2015). Einfluss von Mischungsgradienten auf die Flammenbeschleunigung und die Detonation in Kanälen. Technische Universität München. PhD Thesis.
- [6] Boeck, L. R. (2015). Deflagration-to-Detonation Transition and Detonation Propagation in H₂-Air Mixtures with Transverse Concentration Gradients. Technische Universität München. PhD Thesis.
- [7] Katzy P., Boeck L., Hasslberger J. and Sattelmayer T. (2016). Application of High-Speed OH-PLIF Technique for Improvement of Lean Hydrogen-Air Combustion Modeling. 24th International Conference on Nuclear Engineering. Charlotte, NC, USA.
- [8] Sun Z., Liu F., Bao X. and Liu X. (2012). Research on cellular instabilities in outwardly propagating spherical hydrogen-air flames. International Journal of Hydrogen Energy 37: 7889-7899.